



Switchable Coumarins for Ratiometric pH Sensing

Mercedes M. A. Mazza¹, Francesca Cardano^{1,2,3}, James D. Baker¹, Silvia Giordani^{2,4} and Francisco M. Raymo^{1*}

¹Departments of Chemistry and Biology, Laboratory for Molecular Photonics, University of Miami, Coral Gables, FL, United States, ²Nano Carbon Materials, Istituto Italiano di Tecnologia, Genoa, Italy, ³Department of Chemistry and Industrial Chemistry, University of Genoa, Genoa, Italy, ⁴School of Chemical Sciences, Dublin City University, Glasnevin, Ireland

A fluorescent chromophore and a pH-sensitive heterocycle were integrated within a single covalent skeleton to generate four molecular switches with ratiometric fluorescence response. Upon acidification, the pH-sensitive heterocycle opens to shift bathochromically the absorption and emission bands of the fluorescent chromophore. As a result, an equilibrium between two species with resolved fluorescence is established with fast kinetics in aqueous environments. The relative amounts of the two interconverting forms and their relative emission intensities change with pH, providing the opportunity to probe this parameter ratiometrically with fluorescence measurements. Specifically, the resolved emissions of the two species can be collected in separate detection channels of the same microscope to map their ratio across a labeled sample and reconstruct its pH distribution ratiometrically with spatial resolution at the micrometer level. Additionally, the sensitivity of these molecular switches varies with the nature of the heterocyclic ring and with its substituents, allowing the possibility of regulating their response to a given pH range of interest with the aid of chemical synthesis. Thus, a family of valuable fluorescent probes for ratiometric pH sensing in a diversity of samples can emerge from the unique combination of structural and photophysical properties designed into our innovative molecular switches.

Keywords: coumarins, fluorescence imaging, molecular switches, oxazines, oxazolidines, pH sensors, ratiometric sensors

INTRODUCTION

The quantitative determination of pH in the intracellular space can provide invaluable information on the many processes responsible for regulating cell functions (Weisz, 2003; Boron 2004; Casey et al., 2010). However, the microscaled dimensions of cells in conjunction with the need to ensure minimal structural perturbations restrict the number of analytical methods compatible with these measurements significantly (Loiselle and Casey, 2010; Demuth et al., 2016). In this context, the noninvasive character, micrometer resolution, fast response, and inherent sensitivity of fluorescence measurements (Lakowicz, 2006) and optical microscopy (Murphy, 2001) are particularly convenient. Indeed, membrane-permeable dyes with pH-sensitive emission can be exploited to probe pH in the cytosol and in specific organelles of live cells (Han and Burgess, 2010; Wang et al., 2010; Li et al., 2014; Ni and Wu, 2014; Hou et al., 2017; Specht et al., 2017). Generally, the fluorescence quantum yield of the sensitive molecular probe is designed to change with pH; therefore, the emission intensity measured in a given intracellular region of interest can be correlated quantitatively with pH. Nonetheless, concentration and optical effects can also influence the magnitude of the detected

OPEN ACCESS

Edited by:

Xun Yu,
New York Institute of Technology,
United States

Reviewed by:

Lin Yuan,
Hunan University, China
Maya Thanou,
King's College London,
United Kingdom

*Correspondence:

Francisco M. Raymo
fraymo@miami.edu

Specialty section:

This article was submitted to
Smart Materials,
a section of the journal
Frontiers in Materials

Received: 16 November 2020

Accepted: 07 January 2021

Published: 15 February 2021

Citation:

Mazza MMA, Cardano F, Baker JD,
Giordani S and Raymo FM (2021)
Switchable Coumarins for Ratiometric
pH Sensing.
Front. Mater. 8:630046.
doi: 10.3389/fmats.2021.630046

emission intensity, complicating the quantitative determination of pH. These limitations can be overcome with ratiometric measurements, if the sensitive dye is engineered to produce dual emission in resolved spectral windows (Huang et al., 2018; Bigdeli et al., 2019). Under these conditions, the intensity of one emission can be measured relative to the other in order to eliminate any concentration or optical artifact. In addition to the inherent challenge in designing molecular constructs with dual emission, a further complication in the development of such ratiometric probes arises from the need to adjust their sensitivity to a relatively wide range of pH values. In fact, the pH in the intracellular environment can vary from *ca.* 4 in the acidic lysosomal compartments to as much as *ca.* 8 in the basic mitochondria (Weisz, 2003; Boron 2004; Casey et al., 2010). Thus, modular structural designs that can easily be modified with the aid of chemical synthesis to ensure ratiometric fluorescence response and tunable pH sensitivity would be especially valuable.

Our laboratories identified a mechanism to activate the fluorescence of a coumarin fluorophore in response to pH (Deniz et al., 2012; Swaminathan et al., 2012). It is based on the opening of a 2*H,4H*-benzo [1,3]oxazine (oxazine) ring upon acidification with the concomitant bathochromic shift in the coumarin absorption. Selective excitation of the protonated species then results in intense fluorescence at *ca.* 660 nm. Furthermore, the covalent connection of such a pH-activatable probe to folate ligands allows the activation of fluorescence in acidic endosomal compartments of cancer cells and their discrimination from normal cells (Tang et al., 2017). However, a significant increase in emission intensity is observed only at pH values lower than *ca.* 5. The need to tune the pH sensitivity of this molecular probe and impose ratiometric response on it suggested the possibility of exploring structural modifications of the original oxazine heterocycle and extending these operating principles to 2*H,3H,4H,5H*-[1,3]oxazole (oxazolidine) rings, which are also known to open in response to acidification (Szalóki et al., 2015; Fujioka et al., 2020). This article reports a detailed spectroscopic analysis of four members of this family of molecular switches together with representative imaging experiments in model preparations.

MATERIALS AND METHODS

General Procedures

Chemicals were purchased from commercial sources and used as received. H₂O (18.2 MΩ cm) was purified with a Barnstead International Nanopure Diamond Analytical system. Compounds **1**, **3**, **5–9**, and **11** (Supplementary Figures S1,S2) were prepared according to literature procedures (Wu et al., 2007; Tomasulo et al., 2008; Deniz et al., 2010; Zhang et al., 2015; Mazza et al., 2019; Wang et al., 2020). Electrospray ionization mass spectra (ESIMS) were recorded with a Bruker micrOTOF-Q spectrometer. Nuclear magnetic resonance (NMR) spectra were recorded with a Bruker Avance 400 spectrometer. Absorption spectra were recorded in aerated quartz cells (path length = 1.0 cm) with a Varian Cary 100 Bio spectrometer, equipped with an Agilent Technology Cary Dual Cell Peltier

accessory. Emission spectra were recorded in aerated quartz cells (path length = 1.0 cm) with a Varian Cary Eclipse spectrometer, equipped with a Varian Cary Single Cell Peltier accessory. Fluorescence quantum yields were determined against 9,10-diphenylanthracene (**2Cl** and **4Cl**) and cresyl violet (**2OpH** and **4OpH**), following a literature protocol (Würth et al., 2013). Fluorescence images were recorded with a Leica SP5 laser-scanning confocal microscope. Dynamic light scattering (DLS) measurements were performed with a Malvern Zen1600 apparatus.

Synthesis of 2

Trifluoroacetic acid (TFA, 160 μL, 2.09 mmol) was added dropwise to a solution of **6** (100 mg, 0.32 mmol) and **7** (79 mg, 0.32 mmol) in EtOH (10 ml). The mixture was heated under reflux for 24 h. After cooling down to ambient temperature, the solvent was distilled under reduced pressure and the residue was dissolved in CH₂Cl₂ (50 ml) and washed with NaHCO₃ (5% w/v, 20 ml) and H₂O (20 ml). The organic phase was dried over anhydrous Na₂SO₄ and filtered and the solvent was distilled under reduced pressure. The residue was purified by column chromatography [SiO₂, CH₂Cl₂/MeOH (98:2, v/v)] to give **2** (9%, 15 mg) as a green solid. ESIMS: *m/z* = 538.2359 [M + H]⁺ (*m/z* calcd. for C₃₂H₃₂N₃O₅ = 538.2342); ¹H NMR (400 MHz, CD₃CN): δ (ppm) = 7.81 (s, 1H), 7.64–7.66 (d, 8 Hz, 1H), 7.28–7.35 (m, 2H), 7.17–7.19 (d, 5 Hz, 2H), 6.98–7.09 (m, 2H), 6.82–6.89 (m, 1H), 6.77–6.79 (m, 1H), 6.67–6.72 (m, 2H), 6.51 (s, 1H), 5.02 (d, 19Hz, 1H), 4.78 (d, 19Hz, 1H), 3.41–3.46 (m 4H), 1.52 (s, 3H), 1.16–1.19 (m, 9H); ¹³C NMR (100 MHz, CD₃CN): δ (ppm) = 183.5, 174.3, 137.5, 131.6, 130.5, 129.4, 128.1, 127.5, 126.5, 125.0, 123.1, 122.4, 122.2, 120.4, 109.3, 108.9, 100.1, 80.1, 55.0, 44.6, 38.7, 25.2, 17.8, 11.9.

Synthesis of 4

Palladium(II) acetate (18 mg, 0.07 mmol) was added to a solution of **10** (40 mg, 0.07 mmol) and **11** (20 mg, 0.14 mmol) in Et₃N (20 ml). The mixture was heated under reflux and Ar for 24 h. After cooling down to ambient temperature, the reaction mixture was diluted with CH₂Cl₂ (20 ml) and washed with H₂O (2 × 20 ml). The organic phase was dried over anhydrous Na₂SO₄ and filtered and the solvent was distilled under reduced pressure. The residue was purified by column chromatography [SiO₂, CH₂Cl₂/MeOH (93:7, v/v) and Et₃N (1% v/v)] to give **4** (25%, 10 mg) as a green solid. ESIMS: *m/z* = 563.2888 [M + H]⁺ (*m/z* calcd. for C₃₆H₃₉N₂O₄ = 563.2910); ¹H NMR (400 MHz, CDCl₃): δ (ppm) = 7.60 (s, 1H), 7.44 (d, 8 Hz, 2H), 7.24–7.31 (m, 4H), 6.96 (s, 1H), 6.87–6.92 (m, 2H), 6.75–6.81 (m, 2H), 6.65–6.72 (m, 1H), 6.59 (d, 8 Hz, 1H), 6.51 (s, 1H), 4.30 (m, 1H), 3.81–3.85 (m, 4H), 3.66–3.67 (m, 2H), 3.41–3.49 (m, 4H), 1.49 (s, 3H), 1.25–1.23 (t, 6H), 1.19 (s, 3H); ¹³C NMR (100 MHz, CDCl₃): δ (ppm) = 161.1, 158.8, 155.8, 150.6, 150.5, 140.4, 139.5, 131.6, 130.8, 128.8, 127.8, 127.3, 127.1, 126.8, 126.5, 125.5, 120.2, 117.1, 114.2, 112.1, 110.5, 109.1, 108.9, 97.2, 63.5, 55.3, 50.1, 47.9, 44.8, 28.6, 20.4, 12.5.

Synthesis of 9

2-Bromoethanol (298 μL, 4.21 mmol) was added dropwise to a solution of **8** (1 g, 3.51 mmol) in MeCN (10 ml). The mixture was

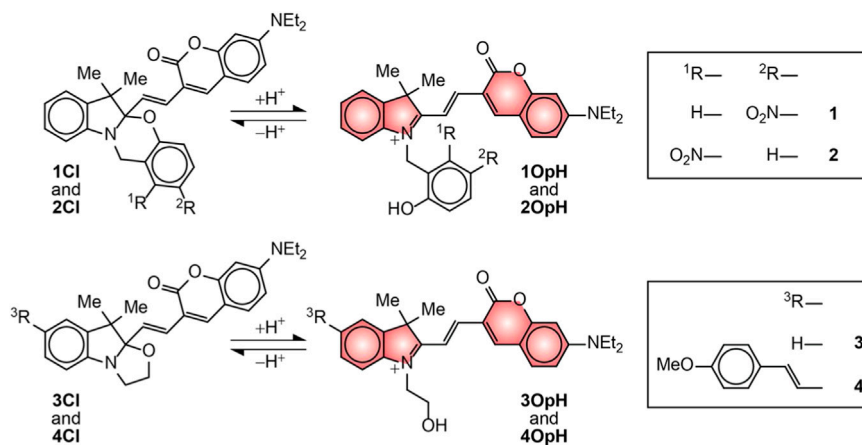


FIGURE 1 | Interconversion of the ring-closed (Cl) and protonated ring-open (OpH) forms of **1–4**.

heated under reflux and Ar for 24 h. After cooling down to ambient temperature, the solvent was distilled under reduced pressure and the residue was dissolved in hexane (10 ml), sonicated for 30 min, and filtered. The residue was dissolved in CH_2Cl_2 (50 ml) and stored in a fridge for 2 h. The resulting precipitate was filtered off, washed with CH_2Cl_2 (20 ml), and dried to give **9** (63%, 910 mg) as a pink solid. ESIMS: $m/z = 330.0349$ $[\text{M}-\text{Br}]^+$ (m/z calcd. for $\text{C}_{13}\text{H}_{17}\text{INO} = 330.0355$); ^1H NMR (400 MHz, CD_3CN): δ (ppm) = 8.13 (s, 1H), 7.99 (d, 8 Hz, 1H), 7.59 (d, 8 Hz, 1H), 4.52 (t, 5 Hz, 2H), 3.99 (t, 5 Hz, 2H), 2.79 (s, 3H), 1.58 (s, 6H).

Synthesis of **10**

TFA (209 μL , 2.65 mmol) was added dropwise to a solution of **7** (100 mg, 0.41 mmol) and **9** (167 mg, 0.41 mmol) in EtOH (8 ml). The mixture was heated under reflux for 24 h. After cooling down to ambient temperature, the solvent was distilled under reduced pressure and the residue was dissolved in CH_2Cl_2 (5 ml). The addition of Et_2O (200 ml) and refrigeration for 12 h resulted in the formation of a precipitate. After filtration, the solid residue was dissolved in aqueous NaHCO_3 (5% w/v, 20 ml) and stirred for 1 h at ambient temperature. The aqueous mixture was extracted with EtOAc (3×40 ml). The organic phase was dried over anhydrous Na_2SO_4 and filtered and the solvent was distilled off under reduced pressure to give **10** as a green solid (22%, 50 mg). ESIMS: $m/z = 557.1293$ $[\text{M} + \text{H}]^+$ (m/z calcd. for $\text{C}_{27}\text{H}_{30}\text{IN}_2\text{O}_3 = 557.1301$); ^1H NMR (400 MHz, CDCl_3): δ (ppm) = 7.59 (s, 1H), 7.45 (d, 8 Hz, 1H), 7.34 (s, 1H), 7.25–7.30 (m, 1H), 6.79 (d, 8 Hz, 1H), 6.64 (d, 17 Hz, 1H), 6.56–6.63 (m, 2H), 6.51 (s, 1H), 4.13 (q, 7 Hz, 1H), 3.76–3.82 (m, 1H), 3.54–3.67 (m, 2H), 3.41–3.46 (m, 4H), 1.42 (s, 3H), 1.27–1.21 (m, 6H), 1.17 (s, 3H).

Preparation of Doped Nanoparticles and Beads

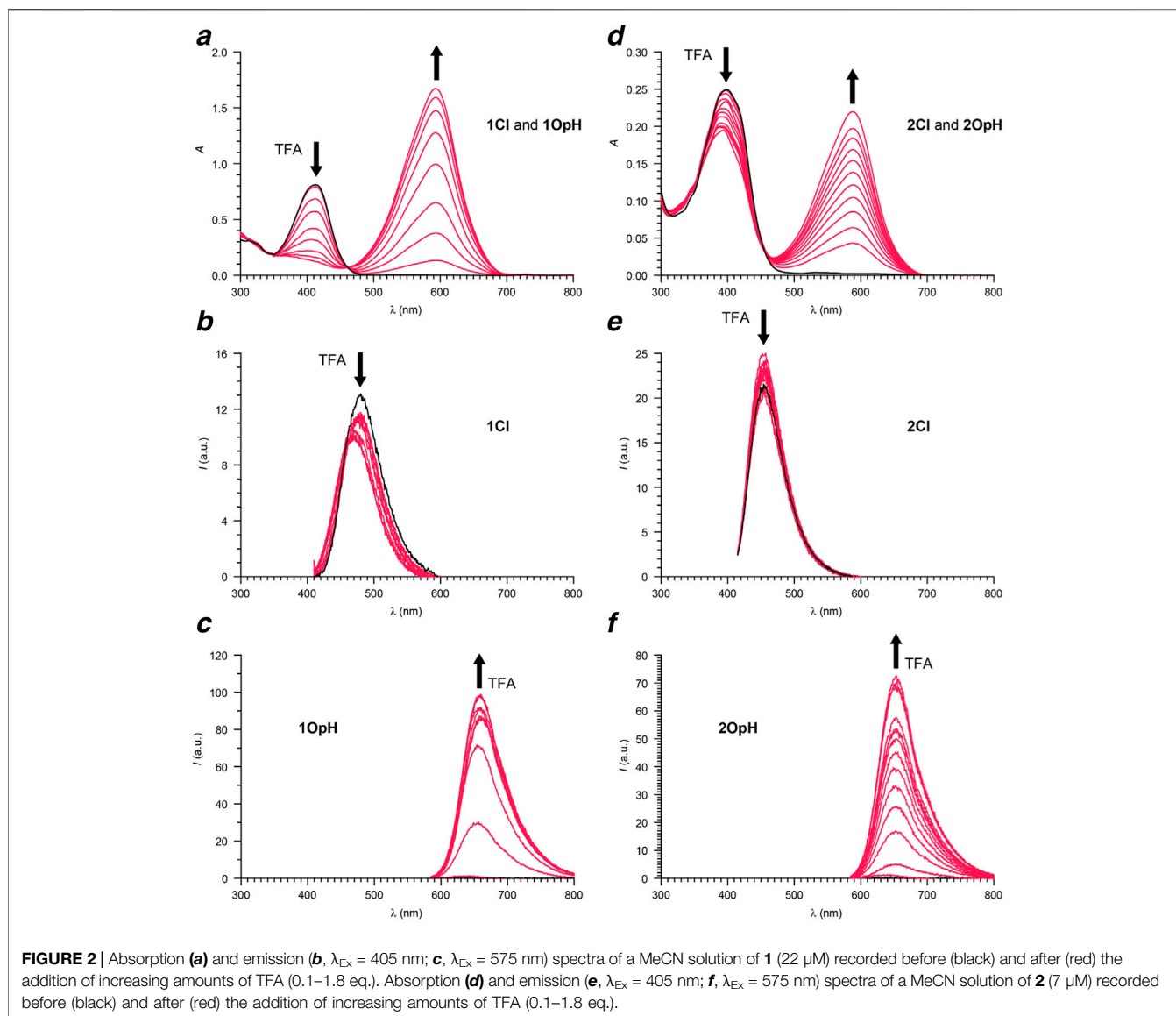
CH_2Cl_2 solutions of **1–4** (0.4–3.1 mM, 10 μL) were individually mixed with a CH_2Cl_2 solution of Pluronic 123 (2.5 mg ml^{-1} , 600 μL) and stirred for 15 min at ambient temperature. The

solvent was distilled off under reduced pressure. The residue was dissolved in H_2O (1 ml) for spectroscopic measurements or in an aqueous solution of sodium alginate (4% w/v, 2 ml) for imaging experiments. DLS measurements revealed the hydrodynamic diameter of the doped polymer nanoparticles to be ca. 80 nm. Droplets of the resulting mixture of sodium alginate and polymer nanoparticles were added to an aqueous solution of CaCl_2 (0.24 M, 750 μL) with a syringe through a 25-gauge needle. Beads with diameters of a few millimeters formed upon contact of the droplets with the CaCl_2 solution. After 2 min, individual beads were suspended in H_2O (500 μL) at different pH, ranging from 7.4 to 4.0, and then transferred to a glass Petri dish.

RESULTS

Compounds **1Cl** and **2Cl** incorporate an oxazine heterocycle and differ in the position of a nitro substituent (**Figure 1**). Compounds **3Cl** and **4Cl** have an oxazolidine heterocycle in place of the oxazine ring and differ in the substituent on 2*H*,3*H*-indole (indole) heterocycle. Compounds **1Cl** and **3Cl** were prepared according to literature protocols (Deniz et al., 2010; Mazza et al., 2019). Compounds **2Cl** and **4Cl** were synthesized in one and three steps, respectively (**Supplementary Figures S1,S2**), and their structural identities were confirmed by high-resolution ESIMS and ^1H NMR spectroscopy.

The absorption spectra (**Figures 2, 3**) of acetonitrile solutions of **1Cl–4Cl** show an intense band at 399–412 nm ($^{\text{Cl}}\lambda_{\text{Ab}}$ in **Table 1**) associated with the coumarin chromophore in all instances. Upon addition of increasing amounts of trifluoroacetic acid (TFA), this absorption decreases in intensity with the concomitant appearance and growth of a new band at 576–594 nm ($^{\text{OpH}}\lambda_{\text{Ab}}$ in **Table 1**). This additional absorption resembles that of model compound **5** (**Supplementary Figure S3**) and is indicative of the opening and protonation of the oxazine or oxazolidine heterocycle to form **1OpH–4OpH**. Indeed, this structural transformation converts

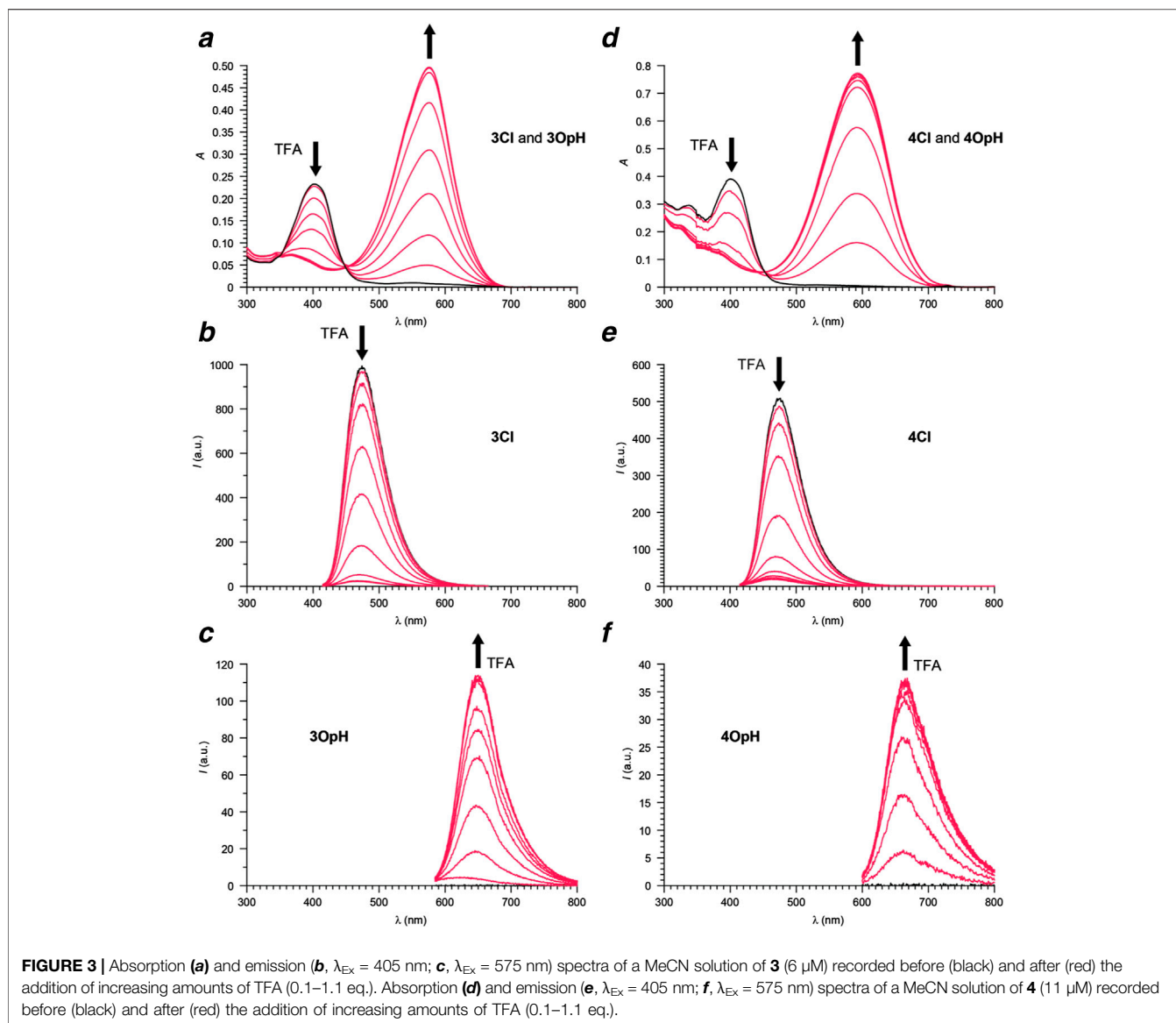


the carbon atom at the junction of the indole and either the oxazine or the oxazolidine heterocycle from sp^3 to sp^2 and brings the coumarin component in conjugation with the resulting 3*H*-indolium cation. As a result of the extended electronic delocalization, the main absorption of the coumarin chromophore shifts bathochromically, in agreement with literature on related compounds (Deniz et al., 2012; Swaminathan et al., 2012; Tang et al., 2017).

The emission spectra (Figures 2, 3) of acetonitrile solutions of **1CI–4CI** reveal an intense band at 454–480 nm ($^{\text{CI}}\lambda_{\text{Em}}$ in Table 1) for the coumarin chromophore in all instances. However, the fluorescence quantum yields ($^{\text{CI}}\phi$ in Table 1) of the oxazine derivatives are significantly lower than those of the oxazolidine counterparts. Upon acidification, this emission band decreases in intensity with the concomitant appearance and growth of a new band at 647–666 nm ($^{\text{OpH}}\lambda_{\text{Em}}$ in Table 1) for **1OpH–4OpH**. Once again, the fluorescence quantum yields ($^{\text{OpH}}\phi$ in Table 1) of the oxazine derivatives are significantly lower than those of the

oxazolidine counterparts. Presumably, electron transfer from the excited coumarin chromophore to the nitro group is responsible for suppressing the ability of the ring-closed and protonated ring-open forms of **1** and **2** to be emitted.

Compounds **1CI–4CI** are relatively hydrophobic and essentially insoluble in aqueous environments. However, they readily dissolve in the presence of appropriate amounts (>1 mg mL^{-1}) of Pluronic 123 and retain their photophysical properties as long as their concentration is maintained in the micromolar regime (<50 μM) to avoid aggregation. Indeed, this particular amphiphilic polymer is known to form micelles capable of capturing hydrophobic molecules in their interior and solubilizing them in aqueous environments (Pitto-Barry and Barry, 2015; Jarak et al., 2020). Consistently, DLS measurements on the resulting solutions indicate the formation of nanoparticles with an average hydrodynamic diameter of ca. 80 nm in all instances. Absorption spectra (Supplementary Figures S4,S5), recorded at different pH values, are consistent with the spectral



changes observed in acetonitrile upon acidification (**Figures 2,3**). Specifically, the absorption band of the ring-closed form at 398–412 nm ($^{\text{Cl}}\lambda_{\text{Ab}}$ in **Table 1**) decreases and that of the protonated ring-open form at 565–608 nm ($^{\text{OpH}}\lambda_{\text{Ab}}$ in **Table 1**) increases upon acidification in all instances. Analyses of the pH dependence of the absorbance at $^{\text{OpH}}\lambda_{\text{Ab}}$ suggest that $\text{p}K_{\text{a}}$ is 5.15 for **1**; 3.51 for **2**; 5.97 for **3**; 5.28 for **4**. Comparison of the values estimated for **1** and **2** demonstrates that the relocation of the nitro group from the *para*- to the *meta*-position, relative to the oxygen atom, on the phenylene ring fused to the oxazine heterocycle hinders protonation and ring opening. Comparison of the values determined for **1** and **3** shows that the transition from an oxazine to an oxazolidine ring has instead the opposite effect.

The pH dependence of the equilibrium between the ring-closed and protonated ring-open forms of **1** to **4**, evident from the absorption spectra, translates into dual emission (**Supplementary Figures S4,S5**). Specifically, the emission band of one species at

465–478 nm ($^{\text{Cl}}\lambda_{\text{Em}}$ in **Table 1**) decreases and that of the other at 647–671 nm ($^{\text{OpH}}\lambda_{\text{Em}}$ in **Table 1**) increases with acidification in all instances, consistently with the behavior observed in acetonitrile (**Figures 2, 3**). As a result, the ratio between the emission intensities of the ring-closed form (I_{Cl}) and that of the protonated ring-open species (I_{OpH}) increase monotonically with a rise in pH. The corresponding plots (**Figure 4**) show that **1**, **3**, and **4** respond to pH predominantly between values of *ca.* 4 and *ca.* 8. The largest change in the magnitude of the ratio between the two emission intensities is observed for **4**. Instead, **2** responds to pH predominantly between values of *ca.* 2 and *ca.* 5, demonstrating that the position of the nitro group on the benzoxazine heterocycle has a pronounced influence on the equilibrium between two interconverting species. These observations suggest that the nature and position of the substituents on the pH-sensitive benzoxazine ring can be exploited to tune the response of these molecular switches.

TABLE 1 | Photophysical parameters for 1–4 [a].

	Solvent	${}^{\text{Cl}}\lambda_{\text{Ab}}$ (nm)	${}^{\text{Cl}}\lambda_{\text{Em}}$ (nm)	${}^{\text{Cl}}\phi$	${}^{\text{OpH}}\lambda_{\text{Ab}}$ (nm)	${}^{\text{OpH}}\lambda_{\text{Em}}$ (nm)	${}^{\text{OpH}}\phi$
1	MeCN	412	480	0.01	594	661	0.02
	H ₂ O	412	472	0.12	593	649	0.53
2	MeCN	399	454	0.02	588	654	0.20
	H ₂ O	401	478	0.02	565	647	0.20
3	MeCN	402	476	0.98	576	647	0.21
	H ₂ O	398	465	0.98	576	644	0.13
4	MeCN	400	476	0.30	594	666	0.13
	H ₂ O	398	466	0.55	608	671	0.08

[a] Wavelengths at the absorption (${}^{\text{Cl}}\lambda_{\text{Ab}}$ and ${}^{\text{OpH}}\lambda_{\text{Ab}}$) and emission (${}^{\text{Cl}}\lambda_{\text{Em}}$ and ${}^{\text{OpH}}\lambda_{\text{Em}}$) maxima and fluorescence quantum yield (${}^{\text{Cl}}\phi$ and ${}^{\text{OpH}}\phi$) of the ring-closed (**Cl**) and protonated ring-open (**OpH**) forms of 1–4. The data listed for OpH in MeCN were measured after the addition of TFA (0.75 eq.) to a solution of the corresponding ring-closed form. The data listed for **Cl** and **OpH** in H₂O were measured in the presence of Pluronic 123 (1.5 mg mL⁻¹) at a pH of 7.5 and 3.0, respectively.

The resolved emission bands of the ring-closed and protonated ring-open forms of 1–4 provide, in principle, the opportunity to probe pH ratiometrically with the acquisition of fluorescence images in separate detection channels of the same microscope. Alginate hydrogels are optimal biocompatible model systems (Seliktar 2012; Rosales and Anseth, 2016; Zhang and Khademhosseini, 2017) to explore these possibilities and allow the identification of appropriate imaging conditions to capture and differentiate the fluorescence of the two interconverting species. Specifically, alginate beads of millimeter dimensions can be doped with nanoparticles of Pluronic 123 containing 4, dispersed in water with a given pH, and imaged. The fluorescence of 4**Cl** can be collected between 450 and 600 nm (yellow channel in Figure 5) and that of 4**OpH** can be recorded between 600 and 770 nm (green channel in Figure 5). The resulting images show a fluorescence increase in the yellow channel (a–d in Figure 5) with a concomitant emission decrease in the green channel (e–h in Figure 5) as the pH rises from 4.0 to 7.4. Plots (i in Figure 5) of the emission intensities measured in the two channels further confirm that they are pH-dependent. In fact, the ratio (j in Figure 5) between them increases monotonically with pH, by analogy with the spectroscopic measurements (Figure 4), providing the opportunity to quantify this parameter ratiometrically. Additionally, storage of the sample at a fixed pH does not cause any change in the detected intensities (Supplementary Figure S6), demonstrating that the sensitive probes neither undergo hydrolytic degradation nor photobleaching under these experimental conditions.

CONCLUSION

The covalent integration of a coumarin chromophore and either an oxazine or an oxazolidine heterocycle within the same molecular skeleton provides the opportunity of assembling molecular switches with ratiometric fluorescence response to pH. The oxazine or oxazolidine heterocycle opens upon acidification to establish an equilibrium between a ring-closed and a protonated ring-open form. In the latter species only, the coumarin chromophore can

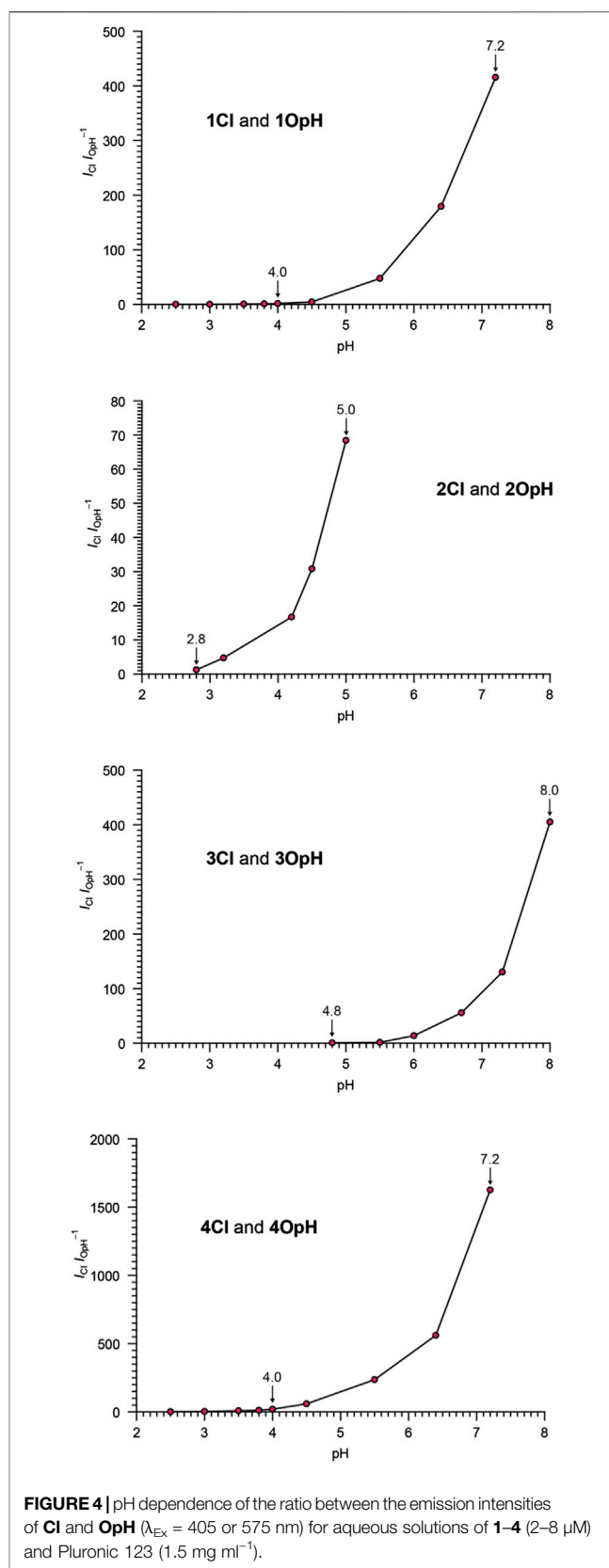


FIGURE 4 | pH dependence of the ratio between the emission intensities of **Cl** and **OpH** ($\lambda_{\text{Ex}} = 405$ or 575 nm) for aqueous solutions of 1–4 (2–8 μM) and Pluronic 123 (1.5 mg mL⁻¹).

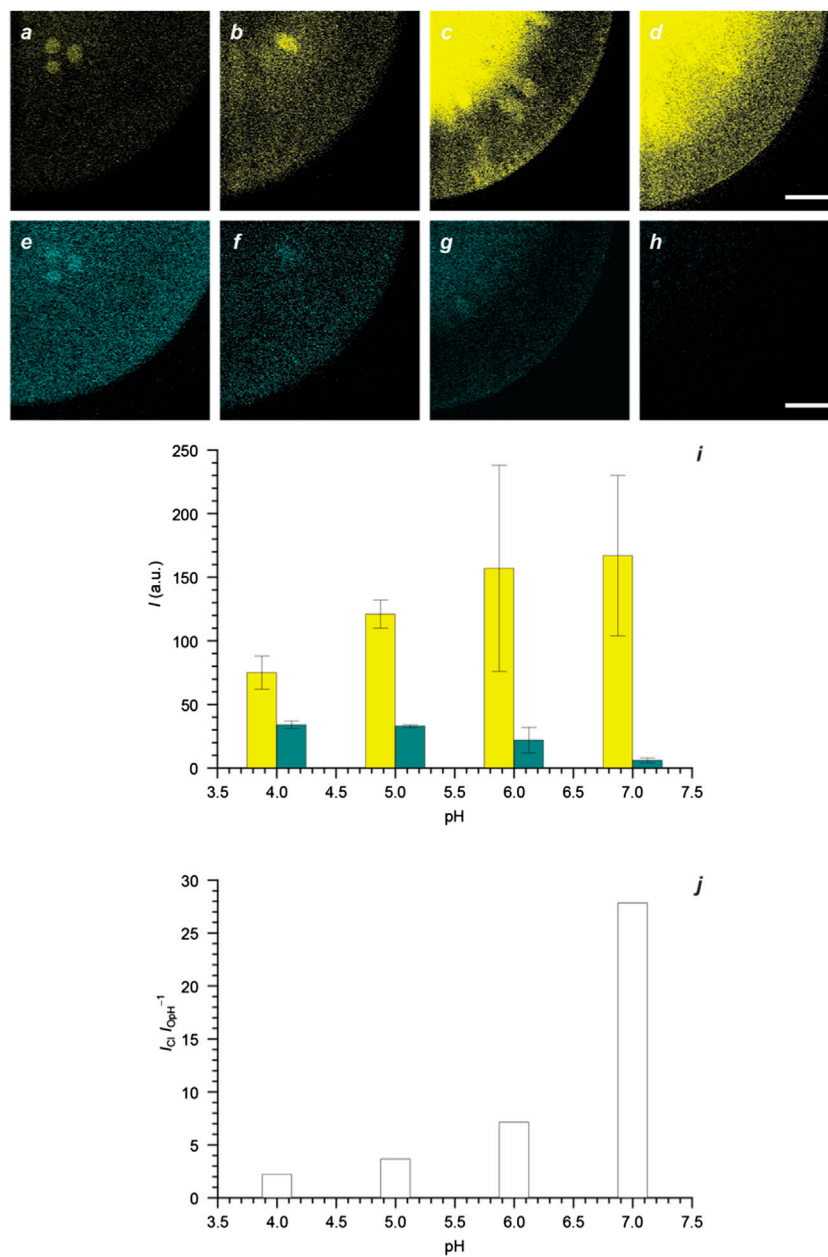


FIGURE 5 | Fluorescence images (scale bar = 200 μm) of four alginate beads doped with Pluronic 123 nanoparticles (1.5 mg mL^{-1}) containing **4** ($5 \mu\text{M}$) and maintained in H_2O at pH of 4.0 (**a** and **e**), 5.0 (**b** and **f**), 6.0 (**c** and **g**), and 7.0 (**d** and **h**) together with the corresponding emission intensities (**i**), integrated across the field of view, and their ratio (**j**) [yellow channel: $\lambda_{\text{Ex}} = 405 \text{ nm}$, $\lambda_{\text{Em}} = 450\text{--}600 \text{ nm}$; green channel: $\lambda_{\text{Ex}} = 561 \text{ nm}$, $\lambda_{\text{Em}} = 600\text{--}770 \text{ nm}$].

extend electronic delocalization over an indolium auxochrome. As a result, the protonated ring-open form is absorbed and emitted at wavelengths that are significantly longer than those where the ring-closed species is absorbed and emitted. This behavior enables the selective excitation of the two interconverting forms at distinct wavelengths and the collection of their emissions in resolved spectral windows. Furthermore, the relative amounts of the two equilibrating species and, hence, their relative emission intensities change with pH. It follows that separate detection channels of the same microscope

can be exploited to collect the fluorescence of the two components independently and reconstruct a ratiometric profile of the pH distribution of any sample of interest labeled with these compounds.

A significant advantage of this family of molecular switches over existing compounds with ratiometric fluorescence response to pH is their synthetic accessibility and versatility. Three synthetic steps from readily available precursors are sufficient to assemble the parent molecular scaffold of both oxazine and oxazolidine derivatives, offering the opportunity to prepare relatively large amounts of these compounds. Additional synthetic

modifications permit the manipulation of the substituents on the indole heterocycle and on the phenylene ring fused to the oxazine ring. These structural manipulations can be exploited to adjust the pH response and, in principle, to introduce hydrophilic chains for aqueous solubility (Cusido et al., 2012) or reactive functional groups for the covalent connection of biomolecules (Cusido et al., 2016; Zhang et al., 2018) or synthetic polymers (Tang et al., 2017). In fact, the fascinating prospect of incorporating targeting agents to direct these molecular switches into specific intracellular components and allow local pH probing can definitely be envisaged. Thus, the combination of photophysical and structural properties that can be engineered into these molecular switches can lead to the realization of versatile fluorescent probes for the intracellular visualization of pH distributions at the microscale with ratiometric imaging schemes.

DATA AVAILABILITY STATEMENT

The original contributions presented in the study are included in the article/**Supplementary Material**; further inquiries can be directed to the corresponding author.

REFERENCES

- Bigdeli, A., Ghasemi, F., Abbasi-Moayed, S., Shahrajabian, M., Fahimi-Kashani, N., Jafarinejad, S., et al. (2019). Ratiometric fluorescent nanoprobe for visual detection: design principles and recent advances - a review. *Anal. Chim. Acta.* 1079, 30–58. doi:10.1016/j.aca.2019.06.035
- Boron, W. F. (2004). Regulation of intracellular pH. *Adv. Physiol. Educ.* 28, 160–179. doi:10.1152/advan.00045.2004
- Casey, J. R., Grinstein, S., and Orlowski, J. (2010). Sensors and regulators of intracellular pH. *Nat. Rev. Mol. Cell Biol.* 11, 50–61. doi:10.1038/nrm2820
- Cusido, J., Battal, M., Deniz, E., Yildiz, I., Sortino, S., and Raymo, F. M. (2012). Fast fluorescence switching within hydrophilic supramolecular assemblies. *Chemistry* 18, 10399–10407. doi:10.1002/chem.201201184
- Cusido, J., Ragab, S. S., Thapaliya, E. R., Swaminathan, S., Garcia-Amorós, J., Roberti, M. J., et al. (2016). A photochromic bioconjugate with photoactivatable fluorescence for superresolution imaging. *J. Phys. Chem. C* 120, 12860–12870. doi:10.1021/acs.jpcc.6b03135
- Demuth, C., Varonier, J., Jossen, V., Eibl, R., and Eibl, D. (2016). Novel probes for pH and dissolved oxygen measurements in cultivations from millilitre to benchtop scale. *Appl. Microbiol. Biotechnol.* 100, 3853–3863. doi:10.1007/s00253-016-7412-0
- Deniz, E., Sortino, S., and Raymo, F. M. (2010). Fluorescence switching with a photochromic auxochrome. *J. Phys. Chem. Lett.* 1, 3506–3509. doi:10.1021/jz101473w
- Deniz, E., Tomasulo, M., Cusido, J., Yildiz, I., Petriella, M., Bossi, M. L., et al. (2012). Photoactivatable fluorophores for super-resolution imaging based on oxazine auxochromes. *J. Phys. Chem. C* 116, 6058–6068. doi:10.1021/jp211796p
- Fujioka, H., Uno, S., Kamiya, M., Kojima, R., Johnsson, K., and Urano, Y. (2020). Activatable fluorescent probes for hydrolase enzymes based on coumarin-hemicyanine hybrid fluorophores with large Stokes shifts. *Chem. Commun.* 56, 5617–5620. doi:10.1039/d0cc00559b
- Han, J., and Burgess, K. (2010). Fluorescent indicators for intracellular pH. *Chem. Rev.* 110, 2709–2728. doi:10.1021/cr900249z
- Hou, J. T., Ren, W. X., Li, K., Seo, J., Sharma, A., Yu, X. Q., et al. (2017). Fluorescent bioimaging of pH: from design to applications. *Chem. Soc. Rev.* 46, 2076–2090. doi:10.1039/c6cs00719h
- Huang, X., Song, J., Yung, B. C., Huang, X., Xiong, Y., and Chen, X. (2018). Ratiometric optical nanoprobe enables accurate molecular detection and imaging. *Chem. Soc. Rev.* 47, 2873–2920. doi:10.1039/c7cs00612h

AUTHOR CONTRIBUTIONS

MA performed spectroscopic measurements. FC synthesized compounds. JB performed imaging experiments. SG supervised synthesis and contributed to manuscript production. FR designed the experiments, analyzed data, and wrote the manuscript.

FUNDING

The National Science Foundation (CHE-1505885) and the Istituto Italiano di Tecnologia (IIT) are acknowledged for financial support.

SUPPLEMENTARY MATERIAL

The Supplementary Material for this article can be found online at: <https://www.frontiersin.org/articles/10.3389/fmats.2021.630046/full#supplementary-material>.

- Jarak, I., Varela, C. L., Tavares da Silva, E., E., T., Veiga, F., Figueiras, A., et al. (2020). Pluronic-based nanovehicles: recent advances in anticancer therapeutic applications. *Eur. J. Med. Chem.* 206, 112526. doi:10.1016/j.ejmech.2020.112526
- Lakowicz, J. R. (2006). *Principles of fluorescence spectroscopy*. New York, NY, United States: Springer
- Li, X., Gao, X., Shi, W., and Ma, H. (2014). Design strategies for water-soluble small molecular chromogenic and fluorogenic probes. *Chem. Rev.* 114, 590–659. doi:10.1021/cr300508p
- Loiselle, F. B., and Casey, J. R. (2010). Measurement of intracellular pH. *Methods Mol. Biol.* 637, 311–331. doi:10.1007/978-1-60761-700-6_17
- Mazza, M. M. A., Cardano, F., Cusido, J., Baker, J. D., Giordani, S., and Raymo, F. M. (2019). Ratiometric temperature sensing with fluorescent thermochromic switches. *Chem. Commun.* 55, 1112–1115. doi:10.1039/c8cc09482a
- Murphy, D. B. (2001). *Fundamentals of light microscopy and electronic imaging*. New York, NY, United States: Wiley-Liss.
- Ni, Y., and Wu, J. (2014). Far-red and near infrared BODIPY dyes: synthesis and applications for fluorescent pH probes and bio-imaging. *Org. Biomol. Chem.* 12, 3774. doi:10.1039/c3ob42554a
- Pitto-Barry, A., and Barry, N. P. E. (2015). Pluronic block-copolymers in medicine: from chemical and biological versatility to rationalisation and clinical advances. *Polym. Chem.* 5, 3291. doi:10.1039/C4PY00039K
- Rosales, A. M., and Anseth, K. S. (2016). The design of reversible hydrogels to capture extracellular matrix dynamics. *Nat. Rev. Mater.* 1, 15012. doi:10.1038/natrevmats.2015.12
- Seliktar, D. (2012). Designing cell-compatible hydrogels for biomedical applications. *Science* 336, 1124. doi:10.1126/science.1214804
- Specht, E. A., Braselmann, E., and Palmer, A. E. (2017). A critical and comparative review of fluorescent tools for live-cell imaging. *Annu. Rev. Physiol.* 79, 93. doi:10.1146/annurev-physiol-022516-034055
- Swaminathan, S., Petriella, M., Deniz, E., Cusido, J., Baker, J. D., Bossi, M. L., et al. (2012). Fluorescence photoactivation by intermolecular proton transfer. *J. Phys. Chem.* 116, 9928. doi:10.1021/jp307787w
- Szalóki, G., Alévêque, O., Pozzo, J.-L., Hadji, R., Levillain, E., and Sanguinet, L. (2015). Indolinooxazolidine: a versatile switchable unit. *J. Phys. Chem. B* 119, 307. doi:10.1021/jp511825f
- Tang, S., Zhang, Y., Thapaliya, E. R., Brown, A. S., Wilson, J. N., and Raymo, F. M. (2017). Highlighting cancer cells with halochromic switches. *ACS Sens.* 2, 92. doi:10.1021/acssensors.6b00592

- Tomasulo, M., Sortino, S., and Raymo, F. M. (2008). Bichromophoric photochromes based on the opening and closing of a single oxazine ring. *J. Org. Chem.* 73, 118. doi:10.1021/jo7017119
- Wang, R., Yu, C., Yu, F., Chen, L., and Yu, C. (2010). Molecular fluorescent probes for monitoring pH changes in living cells. *Trac. Trends Anal. Chem.* 29, 1004. doi:10.1016/j.trac.2010.05.005
- Wang, Y. C., Huang, Y. H., Tsai, H. C., Basha, R. S., and Chou, C. M. (2020). Palladium-catalyzed proaromatic C(alkenyl)-H olefination: synthesis of densely functionalized 1,3-dienes. *Org. Lett.* 22, 6765. doi:10.1021/acs.orglett.0c02241
- Weisz, O. A. (2003). Organelle acidification and disease. *Traffic* 4, 57. doi:10.1034/j.1600-0854.2003.40201.x
- Wu, J. S., Liu, W. M., Zhuang, X. Q., Wang, F., Wang, P. F., Tao, S. L., et al. (2007). Fluorescence turn on of coumarin derivatives by metal cations: a new signaling mechanism based on C=N isomerization. *Org. Lett.* 9, 33. doi:10.1021/ol062518z
- Würth, C., Grabolle, M., Pauli, J., Spieles, M., and Resch-Genger, U. (2013). Relative and absolute determination of fluorescence quantum yields of transparent samples. *Nat. Protoc.* 8, 1535. doi:10.1038/nprot.2013.087
- Zhang, Y., Swaminathan, S., Tang, S., Garcia-Amorós, J., Boulina, M., Captain, B., et al. (2015). Photoactivatable BODIPYs designed to monitor the dynamics of supramolecular nanocarriers. *J. Am. Chem. Soc.* 137, 4709. doi:10.1021/ja5125308
- Zhang, Y. S., and Khademhosseini, A. (2017). Advances in engineering hydrogels. *Science* 356, eaaf3627. doi:10.1126/science.aaf3627
- Zhang, Y., Song, K. H., Tang, S., Ravelo, L., Cusido, J., Sun, C., et al. (2018). Far-red photoactivatable BODIPYs for the super-resolution imaging of live cells. *J. Am. Chem. Soc.* 140, 12741. doi:10.1021/jacs.8b09099

Conflict of Interest: The authors declare that the research was conducted in the absence of any commercial or financial relationships that could be construed as a potential conflict of interest.

Copyright © 2021 Mazza, Cardano, Baker, Giordani and Raymo. This is an open-access article distributed under the terms of the Creative Commons Attribution License (CC BY). The use, distribution or reproduction in other forums is permitted, provided the original author(s) and the copyright owner(s) are credited and that the original publication in this journal is cited, in accordance with accepted academic practice. No use, distribution or reproduction is permitted which does not comply with these terms.